Sizing Optimization Methodology of a Multisource Generator that Harvest the Energy in the Human Environment

Marianne Lossec, Hamid Ben Ahmed, Bernard Multon

SIZING OPTIMIZATION METHODOLOGY OF A MULTISOURCE GENERATOR THAT HARVEST THE ENERGY IN THE HUMAN ENVIRONMENT

M. Lossec[1], H. Ben Ahmed[1], B. Multon[1],

1. SATIE, ENS CACHAN Bretagne, CNRS, UEB, Avenue R. Schuman, 35170 Bruz, France.
e-mail: marianne.lossec@bretagne.ens-cachan.fr

Abstract – This paper focuses on sizing optimization of a multisource generator (here: thermal and photovoltaic) that harvest the energy in the human environment. For this, we introduce energetic models of various elements constituting this generator: thermoelectric and photovoltaic modules, DC-DC boost converter and lithium-ion accumulator. Optimizing the sizing help us to underline the interest or not to introduce an extra conversion stage between the generator and the storage element, and thus to find the optimal architecture of multisource generator, in a given context of resources and consumer load.

Keywords – energy harvesting, energetic modelling, thermoelectric generator, photovoltaic generator, DC-DC converter dual-gate, lithium-ion accumulator, bi-objective optimisation.

1. INTRODUCTİON

The state of art in energy harvesting in the human environment [1,2] highlights the weakness of recoverable power levels necessary to satisfy real applications. In addition, considered resources are often intermittent and fluctuating, it is the case for example of lighting resources. The decorrelation between production and consumption requires a storage element to operate. The hybridization of several sources of energy could help generate more energy on average and reduce the power fluctuations thanks to the possible complementarity of resources which can reduce the required storage capacity or extend its life time.

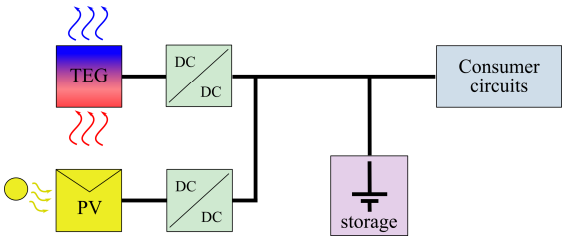

Fig. 1. Multisource generator architecture

This paper focuses on the study of a multisource generator harvesting the thermoelectric energy from the human body and the photovoltaic energy from the ambient light (Fig. 1). The energy from each source is thus converted into electrical energy through a transducer, and can then be adapted and well conditioned with a power electronic converter to maximize the electrical energy produced. However, for low power applications, the addition of such a converter is not always energetically profitable due to generated losses and to performances of the associated generator. The aim of this paper is to propose a method for the sizing optimization of the generator multisource, in a context of known resources, for supplying a consumer circuit where the consumption profile is also fixed. The fundamental parameters of this sizing are the thermoelectric and photovoltaic captation surfaces areas and the storage capacity, technologies being imposed: solid bismuth telluride, amorphous silicon, and lithium-ion. For this, each element of the multisource generator (TE and PV generators, converter and storage element) was modeled and parameterized by the surface area and by the size of the electrochemical element. A bi-objective multi-variable optimization algorithm based on particle swarm optimization [3] was applied to determine the main optimal sizing parameters of the system.

2. MULTİSOURCE GENERATOR MODELİNG

2.1. THERMOELECTRİC GENERATOR MODELİNG

In a context of energy harvesting from the human body, thermal and electrical models of the thermoelectric generator (TEG) are shown in Fig. 2. These benchmark models have been validated [4] from experiments performed with the thermoelectric module TM-450-0.8-3.0, produced by Ferrotec company. This TEG has 450 thermocouples for a surface area of about 30cm^2 and a height of 1.5mm, that is, a density of 15 thermocouples per cm^2.

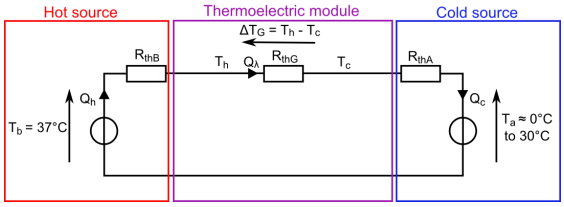

(a)

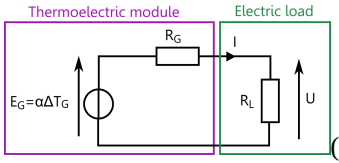

(b)

Fig. 2: Simplified thermal (a) and electrical (b) models of the TEG

The particularity of such a system in the human environment is the very low resource resulting in a low temperature difference between hot and cold sources. According to the powers recoverable, the human body and the environment can be considered as infinite sources of temperature, unaffected by the presence of the TEG. Couplings of the hot and the cold sides with temperatures T_b and T_a are represented by two thermal resistances R_{thB} and R_{thA}. R_{thB} is the thermal resistance between the hot heat source and the hot side of the module. It corresponds to the thermal conduction resistance of the skin and of the thermal contact between the surface of the skin and the hot side of the module. R_{thA} is the thermal resistance between the cold side of the module and the surrounding air. It corresponds to radiation and natural convection of the cold side with ambient air, or to the presence of a heat sink. In addition to these two resistances, the thermal resistance R_{thG} describes heat conduction through all N_{th} thermocouples, which are thermally connected in parallel, and constitute the TEG. From a purely electrical standpoint, the N_{th} thermocouples are electrically connected in series and therefore have a total electrical resistance denoted R_G. Thus, the TEG behaves like an electromotive force (emf) E_G (proportional to the temperature difference at its terminals ΔT_G and to the Seebeck coefficient α) associated to an internal resistance R_G.

Denoted ρ, λ and α_0 the electrical resistivity, the thermal conductivity and the Seebeck coefficient of a thermocouple (average of the two materials), h_A and h_B the heat transfer coefficients on both sides of the TEG, k_f the filling factor of the thermocouples in the TEG, and k_c a coefficient depending on electrical operating point of the TEG (equal to ¼ in the case of an electrical impedance matching), we can express the emf E_G and the recoverable power P_e at the output of the TEG as:

$$E_G = N_{th}\alpha_0 \frac{l_{th}}{l_{th}+k_{env}}\left(T_b - T_a\right)$$

$$P_e = \frac{k_c k_f \alpha_0^{\,2}}{4\rho}\frac{S_{th} l_{th}}{\left(l_{th}+k_{env}\right)^2}\left(T_b - T_a\right)^2 \qquad (1)$$

$$\text{with} \quad k_{env} = \lambda k_f \left(\frac{1}{h_B}+\frac{1}{h_A}\right)$$

When optimizing the sizing, the parameters considered are the leg length l_{th} and the surface area S_{th} of the TEG (Fig. 3). We assume a constant surface density of thermocouples (15 per cm^2) and thus a value of N_{th} proportional to the surface area S_{th}. In addition, the ambient temperature T_a is a variable parameter defining the primary thermal resources. As for the temperature T_b, it is considered as constant.

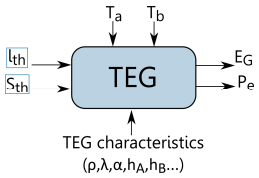

Fig. 3: Inputs, outputs and parameters of the TEG model

2.2. PHOTOVOLTAÏC GENERATOR MODELİNG

In the study of the considered multisource generator, we assume that the carrier of the multisource generator will be more often exposed to indoor lighting than outdoor lighting. Under these conditions, the amorphous silicon technology is an attractive solution because its performance degrades less than other PV technologies to low light, especially in artificial light. In the following, all experiments shown were performed with amorphous silicon photovoltaic modules produced by Solems compagny (reference 07/048/032, the cell sides measure 48mm x 32mm).

The identification of an electrical and energetic model is realized from measurement points. For this, we developed a system of characterization and acquisition for varying the output current of the cell over a wide range. Using a fluorescent lamp whose distance from the cell is varied and a light meter measuring the lighting in the plane of the cell, we were able to measure the current-voltage (I_{PV}/V_{PV}) and then power-voltage (P_{PV}/V_{PV}) graphs, for different lightings E_{PV} in a range from 700 to 4000 lux (scatterplot in Fig. 3). The identification of the mathematical model parameters described by equation (2) is performed by the method of least squares.

$$I_{PV} = a_{PV} + \frac{1}{b_{PV} + c_{PV} V_{PV}^{\,2}} \qquad (2)$$

As the parameters a_{PV}, b_{PV} and c_{PV} evolve according to the lighting E_{PV}, we have modeled them, always by the method of least squares, by the following polynomials:

$$\begin{aligned} a_{PV} &= a_1 E_{PV} + a_0 \\ b_{PV} &= b_3 E_{PV}^{\,3} + b_2 E_{PV}^{\,2} + b_1 E_{PV} + b_0 \\ c_{PV} &= c_3 E_{PV}^{\,3} + c_2 E_{PV}^{\,2} + c_1 E_{PV} + c_0 \end{aligned} \qquad (3)$$

In Fig. 4, are presented the theoretical and experimental graphs obtained, the solid lines correspond to the PV cell model described by equations (2) and (3).

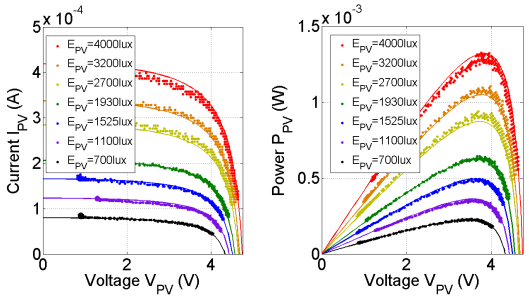

Fig. 4: Theoretical and experimental current vs voltage (left) and power vs voltage (right) graphs for different lightings E_{PV}

Note that the produced power by PV generator depends on the voltage at its terminals, so, in the case where the PV generator is directly connected to the accumulator, the power depends on its state of charge. The only sizing parameter of the PV generator is its surface area S_{PV}, and the parameter defining the primary photovoltaic resource is the lighting E_{PV} (Fig. 5).

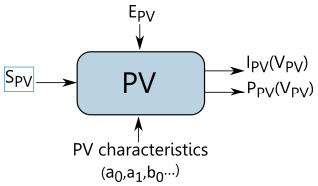

Fig.5: Inputs, outputs and parameters of the PV generator model

2.3. DC-DC CONVERTER MODELİNG

The DC-DC boost converter under study is a very low voltage converter with two dual-gate MOS transistors, one used for the transistor function and the other to replace the diode thereby significantly reduces conduction losses. The dual-gate MOS can extend the range of the converter efficiency thanks to a change of operating mode in low power. The difference between the two gates is the controlled area: we denote k_G, higher than 1, the ratio between the two electrode areas. The gate charge Q_G is proportional to the area while the channel resistance r_{dson} is inversely proportional. Thus, the solution adopted by the LTC3537 converter is to drive the gate with a small area at low powers, where the losses related to the control gate become predominant, and to drive the gate with a large area at high powers. This concept is described in [5]. We denote k_M a coefficient equal to k_G when the driven gate area is the smallest, and equal to 1 in the other case. The switching operation of MOS transistors is associated with losses of different natures that we take into account in the converter modeling: conduction (P_{cond}), switching (P_{SW}) and control gate (P_G). They are expressed as follows:

$$\begin{aligned} P_{cond} &= k_M r_{dson} I_{IN}^{\,2} \\ &= k_M \left(\alpha r_{nmos} + (1-\alpha) r_{pmos}\right) I_{IN}^{\,2} \\ P_{SW} &= f V_{OUT} I_{IN} t_{SWeq} \\ P_G &= f\left(\left(Q_{gn} + Q_{gp}\right)/k_M\right) V_G \\ &= 2f\left(Q_{Geq}/k_M\right) V_{OUT} \end{aligned} \qquad (4)$$

Note that given the specific driver of MOS transistors, switching losses do not depend on the gate area. In addition to losses related to MOS transistors, we also take into account the copper losses modeled by the series resistance r_L of the inductance. Fig. 6 illustrates the electrical model of the DC-DC converter.

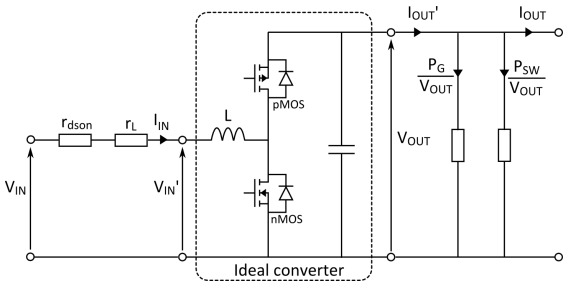

Fig. 6: Electrical model of the DC-DC converter

For the LTC3537, we identified a factor k_G equal to 10. Fig. 7 shows the simulated efficiency curves associated with experimental measurements, for an output voltage V_{OUT}=3.3V.

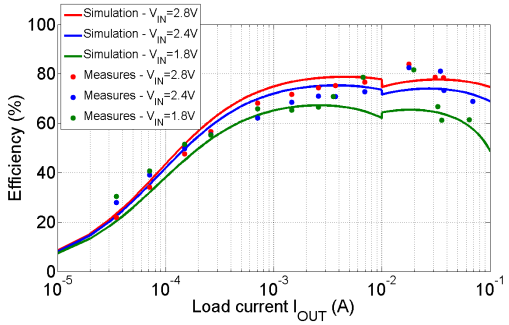

Fig. 7: Simulated and measured efficiency curves of the LTC3537 for V_{OUT} = 3.3 V

In Fig. 7, we can easily observe the effect of switching gate area for a load current of 10 mA, which is characterized by an irregularity on the efficiency curve.

In the sizing optimization of the multisource generator, the parameters of DC-DC converter does not vary, no sizing parameter is then defined.

2.4. LİTHİM-İON ACCUMULATOR MODELİNG

As a first approximation, the lithium battery can be modeled electrically by an electromotive force E_{sto} depending on its state of charge, denoted SOC, in series with an internal resistance R_{sto} also depending on its state of charge (Fig. 8).

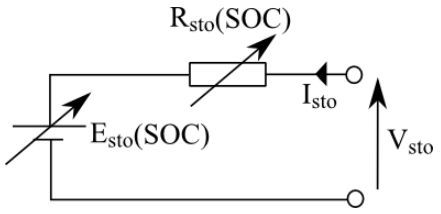

Fig. 8: Electrical model of a lithium-ion battery (receiver convention i.e. $I_{sto}>0$ when charging)

This modeling takes into account the copper losses in the accumulator but also the faradic efficiency. This efficiency reflects the ability of the cell to convert electrical energy into chemical energy during charging, and vice-versa during discharge. It is generally considered close to unity for lithium-ion technology but we still tried to quantify it. We note C_{stoMax} the maximum capacity of an accumulator with a nominal capacity C_{Nom}. The faradic efficiency in charge and in discharge is defined as follow:

$$\eta_f = \frac{C_{sto}}{C_{stoMax}} = \frac{\int |I_{sto}|\,dt}{C_{stoMax}} \qquad (5)$$

The objective of this modeling is to identify experimentally the function $E_{sto}=f_{Esto}(SOC)$, and the functions $C_{sto}=f_{Csto}(|I_{sto}|)$ and $R_{sto}=f_{Rsto}(SOC)$ in charge and in discharge. All experiments presented were performed with a lithium ion polymer accumulator, produced by Ultralife Battery compagny, with a nominal capacity C_{Nom} = 140 mAh.

For the function $E_{sto}=f_{Esto}(SOC)$, the accumulator being initially charged (E_{sto}=4.2V), we discharge it in steps at a constant current of C/10, i.e. I_{sto} = 14 mA. Then, at each step, after a relaxation time of 24h, we measured the voltage across its terminals. We thus discharged every days the accumulator of 5% of its state of charge, and that during 20 days. The result of this test is shown in Fig. 9.

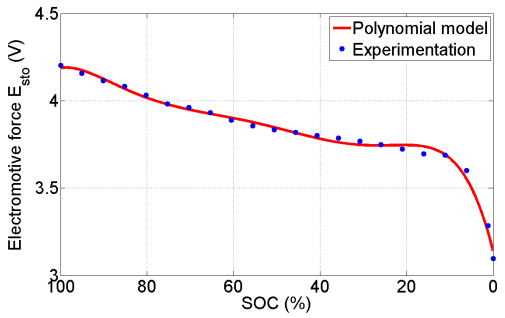

Fig. 9: Experimental measurement and model of the emf E_{sto} according to the state of charge (SOC)

From these measurements, we have mathematically modeled the emf E_{sto} by a 6th-order polynomial function (solid line in Fig. 9).

With regard to the functions $C_{sto}=f_{Csto}(I_{sto})$ and $R_{sto}=f_{Rsto}(SOC)$, we conducted several tests in charge and in discharge for constant currents ranging from C/2 (I_{sto}=70mA) to C/7 (I_{sto}=20mA), and measured by the precision power meter LMG-310 (Zimmer), the current I_{sto} and the voltage V_{sto}. The calculation of the capacity C_{sto}, i.e. the charge stored during a charge or the charge restored during a discharge, is simple: we just have to integrate, with respect to the time, the current I_{sto} measured by the power meter. Then, thanks to the equation (5), we can deduce the faradic efficiency. The results are shown in Fig. 10

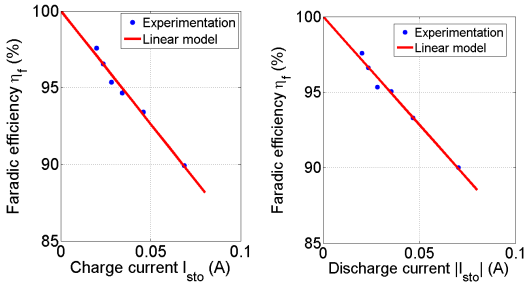

Fig. 10: Evolution of the faradic efficiency η_f according to the current I_{sto} in charge (left) and discharge (right)

Whether in charge or in discharge, we modeled the evolution of the faradic efficiency, and therefore the capacity, by a linear function with a negative coefficient as:

$$C_{sto} = \eta_f C_{stoMax} = K_{Csto0} - K_{Csto1}|I_{sto}| \qquad (6)$$

For the function $R_{sto}=f_{Rsto}(SOC)$ in charge and in discharge, we modeled the average resistance of the conducted tests in charge and in discharge by a 10th-order polynomial function (Fig. 11).

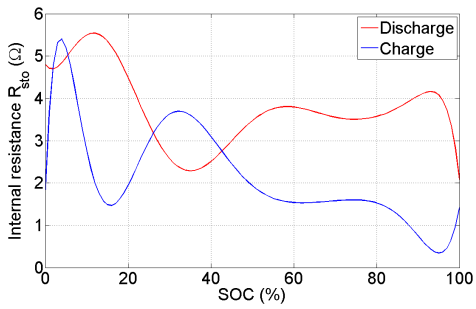

Fig. 11: Evolution of the resistance $R_{sto,}$ in charge and discharge, according to the SOC (identified model)

The model described above is valid for a reference accumulator with a nominal capacity C_{ref} = 140 mAh. However, in order to simulate the energy behavior of lithium-ion accumulator in a wide range of capacity, we developed a generic model thanks to the model of the reference accumulator. Thus, for an accumulator with a nominal capacity $C_{Nom,}$ we have:

$$C_{sto} = K_{Csto0}\frac{C_{Nom}}{C_{ref}} - K_{Csto1}\frac{C_{ref}}{C_{Nom}}|I_{sto}|$$
$$R_{sto} = \frac{C_{ref}}{C_{Nom}} f_{Rsto}(SOC) \quad (7)$$

Thus, given C_{Nom} and $I_{sto}(t)$, these equations enable the determination of the losses in the storage element and the tension $V_{sto}(t)$ at its terminals. In the sizing optimization of the multisource generator, the accumulator capacity C_{Nom} is a sizing parameter (Fig. 12).

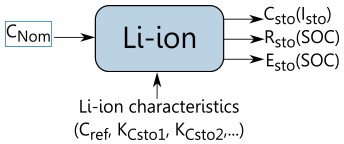

Fig. 12: Inputs, outputs and parameters of the lithium-ion accumulator model

3. SIZING OPTIMIZATION

3.1. OPTIMIZATION METHODOLOGY

In order to size a generator multisource harvesting energy in the human environment, we introduced a bi-objective multi-variable optimization algorithm based on particle swarm optimization [3] and Pareto dominance. This algorithm, called MOPSO, has been implemented in a Matlab environment in our laboratory and has already been used for another application [6]. Thanks to energetic models of different components of this mutisource system, we can simulate the evolution of energy flows over time, each simulation last an hour (t_f = 1h). For each optimization, the profiles of energy resources (lighting E_{PV} and temperature Ta) and of the load are fixed; they are illustrated in Fig. 13.

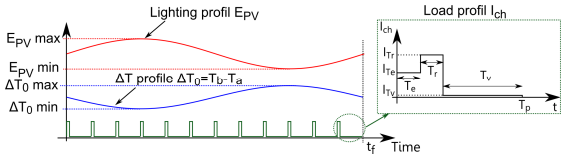

Fig. 13: Profiles of thermal and photovoltaic production and load consumption

The two competing optimization objectives considered are the minimization of the total surface area of the generators $S_T = S_{PV}+S_{th}$ and the nominal capacity of the accumulator C_{Nom}. In addition, we defined three constraints on the storage element:

- 10%<SOC<100%
- $SOC(t=t_f)=SOC(t=0)$

Note that SOC(t=0) is an optimization parameter.

Fig. 14 represent the optimization strategy and specifies the five optimization parameters considered that are C_{Nom}, SOC(t=0), S_{PV}, S_{th} and l_{th}. The result is presented as a Pareto front in terms of objectives that are to minimize C_{Nom} and $S_T = S_{PV}+S_{th}$.

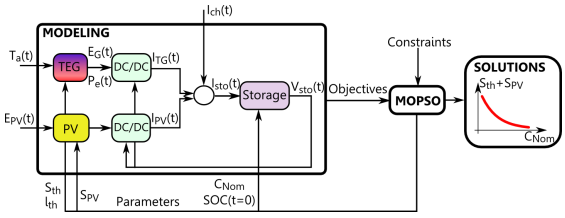

Fig. 14: Implementation of the optimization algorithm

For all optimizations presented in this paper, the load profile, similar to a consumer profile of a communicating sensor, is the same with the values defined in Table 1 (see Fig. 13).

Current	Time
I_{Te}=15mA	T_e=0.5s
I_{Tr}=20mA	T_r=0.5s
I_{Tv}=1µA	T_v=299s

Table 1: Current and time values of load profile (cf. Fig. 13)

Moreover, for the different optimizations that follow, some parameters were constants; they are defined in Table 2.

	Parameters	Values
TEG parameters	α_0	267 µV.K^{-1}
	λ	0.77 W.m^{-1}.K^{-1}
	ρ	20 µΩ.m
	k_f	0.6
	h_B	25 W.m^{-2}.K^{-1}
	h_A	13 W.m^{-2}.K^{-1}
	T_b	37°C
Converter parameters	f	2.2 10^{6} Hz
	t_{SWeq}	70 10^{-9} s
	Q_{Geq}	2 10^{-10} C
	r_L	0.6 Ω
	r_{nmos}	0.4 Ω for V_{OUT}=3.3V 0.3 Ω for V_{OUT}=5V
	r_{pmos}	0.6 Ω for V_{OUT}=3.3V 0.4 Ω for V_{OUT}=5V

Table 2: Constant parameters for the optimizations

3.2. Optimization of the thermoelectric generator alone

In this subsection, we study only the thermoelectric generator, connected to a storage element and a consumer load. Considering the temperature profile T_a described in Fig. 13, we optimized the sizing of the system when the TEG is connected or not to a DC-DC converter. Two temperature profiles were studied: 10<T_a<15 and 15<T_a<20. The results are shown in Fig.15.

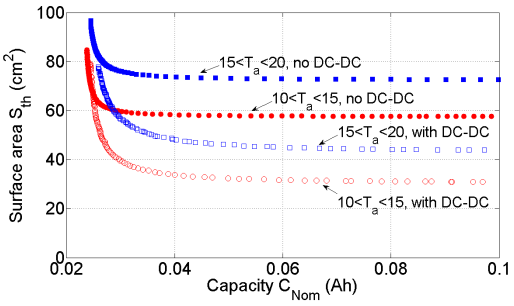

Fig. 15: Optimization results with thermoelectric generation

This first result shows the advantage of adding a DC-DC converter between the TEG and the storage element: the optimization solutions are better with the presence of a converter. Despite these losses, the benefit of such a converter is to raise the low voltage output of the TEG to be able to connect it to an accumulator with a voltage between 3.5V and 4.2V depending on its state of charge. To connect directly the TEG to the accumulator, the voltage of the TEG must be sufficiently high, which involves a large number of thermocouple N_{th} and therefore a large surface area S_{th}. An alternative is to integrate a maximum of thermocouples in the TEG, so to use other technologies, such as those of Micropelt or Thermolife companies, which have a density of about 50 thermocouples per mm^2 [7].

Furthermore, Fig. 15 shows that there is firstly a minimum capacity value and secondly a minimum surface area S_{th} below which the consumption profile imposed can not be satisfied.

3.3. Optimization of the photovoltaic generator alone

We then performed the same optimizations, this time with a photovoltaic generator, for two lighting profiles: 300 <E_{pv} <1400 and 300 <E_{pv} <700 (cf Fig. 13). The results are shown in Fig. 16.

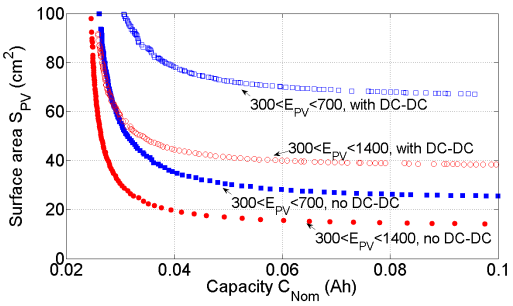

Fig. 16: Optimization results with photovoltaic generation

These results show, unlike the previous case, that adding an extra conversion stage is not advantageous. The improvement of the power produced by the PV generator with the converter MPPT does not compensate the losses generated by the latter. However, the converter used is not necessarily well optimized for these powers. In practice, the converter should be parameterized in order to vary these parameters depending on its use.

Moreover, again, minimum values of capacity and surface area are highlighted.

3.4. Optimization of the multisource generator

After optimizing the sizing of each generator separately, we focused on optimizing a multisource generator including a thermoelectric generator with a DC-DC converter, and a photovoltaic generator without a DC-DC converter. For this optimization, the ambient temperature T_a varies between 10 and 15 °C, and the lighting E_{PV} varies between 300 and 700 lux. The result of this optimization is shown in Fig. 17 (red dots). On this figure, we also redraw the solutions of the previous optimizations: in solid line, the solutions with the photovoltaic generator alone (without a DC-DC converter), and in dotted line, the solutions with thermoelectric generator alone (with a DC-DC converter).

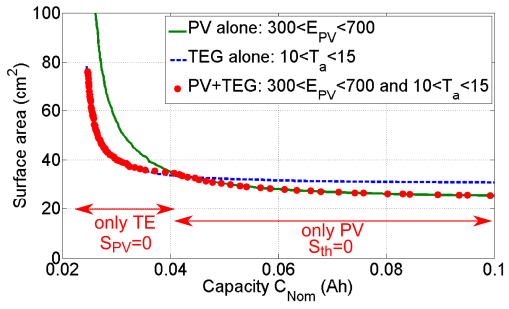

Fig. 17: Optimization results with mutisource generation

In this particular context, the solutions found by the optimization algorithm are always single-source solutions. Thus, for a storage capacity below a certain value (here 0.04 Ah), the minimization of $S_T = S_{PV}+S_{th}$ leads to $S_{PV}=0$ and $S_{th}=S_{th\ opt}$ identical to the single-source case. In Fig. 17, the two curves (dotted line for the TEG alone and red dots for the multisource generator) are merged. For a highter capacity, the configuration minimizing $S_T=S_{PV}+S_{th}$ is the one where $S_{th}=0$. Therefore, for the production and consumption profiles considered, the choice of the production mode depends on the importance of the storage cost in the overall system cost. If this cost is low, PV production is preferred. If the storage cost is, on the opposite, dominant, then thermal production is preferred. A hybrid solution is not optimal here. However, these results and conclusions must be moderated because only one example of production and consumption has been studied. A sensitivity analysis focusing on these profiles or a formalization of this problem is therefore necessary to conclude on the relevance of the hybridization of production modes.

4. Conclusion

In this article we have presented energetic models of different elements which can constitute a multisource generator. The thermoelectric generator is modeled by an emf and an internal resistance depending on thermal resources and on the thermo-electric coupling with the environment. Thanks to the modeling of the PV generator, we are able to determine the generator graphs according to light resources. The developed model of DC-DC converter, with dual-gate MOS, takes into account the losses by conduction, switching and gate drive. The storage element, here a lithium-ion accumulator, is represented by an emf and an internal resistance both depending on the state of charge. All of these developed energetic models have enabled the simulation of the multisource generator on a given cycle (resources and load profiles fixed), and then the sizing optimization. We have shown that for this power level, specific to scavengers in human environment, a DC-DC conversion stage is energetically useful when using a TEG but not for the PV generator. However, note that the PV generator is particularly well adapted to the voltage of a lithium element, and the converter sizing could probably be improved. Finally, the need for hybridization of production modes could not be shown in the simplified case treated, a sensitivity analysis focusing on production and consumption profiles is necessary.

5. References

[1] A. Harb, Energy harvesting: State-of-the-art, Renewable Energy, 2010, doi:10.1016/ j.renene.2010.06.014

[2] E. Cantatore, M. Ouwerkerk, Energy scavenging and power management in networks of autonomous microsensors, Microelectronics Journal, vol. 37, no. 12, pp. 1584-1590, 2006.

[3] M. Reyes-Sierra, C.A. Coello Coello, Multi-Objective Particle Swarm Optimizers: A Survey of the state-of-the-Art, International Journal of Computational Intelligence Research, Vol. 2, No. 3, pp. 287-308, 2006

[4] M. Lossec, B. Multon, H. Ben Ahmed, C. Goupil, Thermoelectric generator placed on the human body: system modeling and energy conversion", EPJAP, 52, 11103, Sept. 2010.

[5] R. Williams, W. Grabowski, A. Cowell, M. Darwish, and J. Berwick, The dual-gate W-switched power MOSFET: a new concept for improving light load efficiency in DC/DC converter, in Proc. Int. ISPSD, 1997, pp. 193-196.

[6] J. Aubry, H. Ben Ahmed, B. Multon, Bi-Objective Sizing Optimization of a PM Machine Drive on an Operating Profile, in Proc. Int. ICEM 2010, Rome

[7] M. Lossec, B. Multon, H. Ben Ahmed, Sizing Optimisation with Thermal and Electrical Matching of a Thermogenerator placed on the Human Body, in Proc. Int. IREED 2011, Lille